Research Square

Preprints are preliminary reports that have not undergone peer review.
They should not be considered conclusive, used to inform clinical practice,
or referenced by the media as validated information.

IGF2 associated PI3K signaling shapes temozolomide sensitivity in glioblastoma

Wenrui Jin
School of Pharmacy, Yantai University
Zefeng Song
Shandong Laboratory of Yantai Drug Discovery, Bohai Rim Advanced Research Institute for Drug Discovery
Xiaojing Zhu
Shandong Laboratory of Yantai Drug Discovery, Bohai Rim Advanced Research Institute for Drug Discovery
Yutong Xing
Shandong Laboratory of Yantai Drug Discovery, Bohai Rim Advanced Research Institute for Drug Discovery
Kai Xu
Department of Neurosurgery, Central Hospital of Dalian University of Technology
Haoran Geng
Shandong Laboratory of Yantai Drug Discovery, Bohai Rim Advanced Research Institute for Drug Discovery
Peng Zhang
School of Pharmacy, Yantai University
Chengjun Wu
School of Life and Health Sciences, Qingdao Central Hospital, University of Health and Rehabilitation Sciences
Zhenyong Wu
wuzhenyong@simm.ac.cn

Shandong Laboratory of Yantai Drug Discovery, Bohai Rim Advanced Research Institute for Drug Discovery

---

Research Article

Keywords: Glioblastoma, IGF2, PI3K signaling

Posted Date: March 8th, 2026

DOI: https://doi.org/10.21203/rs.3.rs-8542364/v1

License: This work is licensed under a Creative Commons Attribution 4.0 International License.
Read Full License

Additional Declarations: No competing interests reported.

Abstract

Resistance to temozolomide (TMZ) remains a major obstacle in glioblastoma (GBM) therapy and cannot be fully explained by canonical DNA repair mechanisms alone. Here, by integrating large scale transcriptomic datasets with machine learning based prioritization and functional validation, we identify insulin-like growth factor 2 (IGF2) as a key molecular hub linking tumor metabolic reprogramming to chemoresistance in GBM. Differential expression analysis of TCGA-GBM and GTEx normal brain tissues, followed by intersection with chemoresistance- and metabolism-related gene sets, yielded candidate cross-hub genes that were further refined using LASSO regression and XGBoost modeling. Among these, IGF2 emerged as the gene consistently associated with poor overall survival across both TCGA and independent CGGA cohorts, which higher expression was validated by human GBM tissues. Functionally, IGF2 silencing suppressed GBM cell viability, promoted apoptosis, and significantly enhanced TMZ sensitivity. Transcriptomic profiling revealed that IGF2 knockdown broadly downregulated resistance associated gene programs and disrupted pathways involved in cellular metabolism, DNA damage response, and cell cycle regulation. Notably, both patient stratification analyses and IGF2 knockdown induced transcriptional changes converged on the PI3K signaling axis. Pharmacological inhibition of PI3K using Paxalisib further potentiated TMZ efficacy, with combination treatment producing the strongest anti-proliferative effects. Together, **these findings indicate a link** between IGF2-associated PI3K signaling, metabolic reprogramming, and TMZ resistance in GBM, providing a rationale for further exploration of this pathway as a therapeutic target

Introduction

Glioblastoma (GBM) is the most aggressive primary malignancy of the central nervous system in adults and is characterized by extensive infiltrative growth, pronounced biological heterogeneity, and an exceptionally high recurrence rate(.Omuro and DeAngelis 2013, Wu et al. 2021). Despite standard-of-care treatment consisting of maximal safe surgical resection followed by radiotherapy and temozolomide (TMZ) chemotherapy, the overall prognosis of GBM patients remains dismal, with most cases eventually experiencing tumor recurrence(.Weller et al. 2013). As the frontline chemotherapeutic agent, TMZ induces DNA damage that triggers tumor cell death(.Roos et al. 2007); however, intrinsic and acquired resistance to TMZ is widespread in clinical practice and represents a critical barrier to durable therapeutic benefit.

Traditional studies of TMZ resistance have largely focused on DNA repair mechanisms, particularly the role of O6-methylguanine-DNA methyltransferase (MGMT) promoter methylation status as a predictive biomarker of TMZ response(.Li et al. 2025,). Nevertheless, accumulating clinical evidence indicates that TMZ resistance cannot be fully explained by MGMT-mediated repair alone. Many patients with MGMT promoter methylation still develop resistance, whereas a subset of unmethylated tumors display transient sensitivity(.Hegi and Stupp 2015, Kitange et al. 2009). These observations suggest that TMZ resistance arises from broader tumor-intrinsic adaptive programs involving signaling network remodeling, enhanced stress tolerance, and metabolic state reconfiguration.

Metabolic reprogramming is a hallmark of GBM biology(.Cortes Ballen et al. 2024). GBM cells dynamically adjust glucose, lipid, and amino acid metabolism to meet bioenergetic and biosynthetic demands and to survive under hypoxia, nutrient deprivation, and therapeutic stress(.Agnihotri and Zadeh 2016). Alterations in metabolic state not only support tumor growth and survival but also reshape transcriptional programs and influence drug sensitivity(.Xu et al. 2023). Despite increasing recognition of the importance of metabolism in therapy resistance, key molecular determinants that simultaneously link metabolic reprogramming and TMZ resistance remain incompletely defined.

Insulin-like growth factor 2 (IGF2) is a secreted growth factor implicated in cellular growth, nutrient utilization, and adaptation to the tumor microenvironment(.LeRoith et al. 2021). Aberrant upregulation of IGF2 has been reported in multiple malignancies, including breast(.Wang et al. 2025), colorectal(.Zhang et al. 2023), and lung cancers(.Jang et al. 2024), and is often associated with tumor progression and unfavorable outcomes. Although IGF2 has been linked to oncogenic signaling and metabolic regulation(.Livingstone 2013), whether IGF2 is associated with TMZ resistance and metabolism-related transcriptional programs in GBM, and which pathways may be involved, remains unclear.

In this study, we integrated large-scale TCGA datasets with in vitro experimental validation to identify and characterize candidate molecular regulators linking metabolic reprogramming and chemoresistance in GBM. Through differential expression analysis, gene set intersection, and machine learning based prioritization using LASSO and XGBoost, we identified IGF2 as a key candidate gene and validated its prognostic relevance in both TCGA and CGGA cohorts. We systematically assessed IGF2 expression patterns, clinical associations, and functional relevance in patient samples and GBM cell models. Furthermore, guided by pathway enrichment analyses highlighting PI3K related transcriptional features, we evaluated cellular responses to TMZ, the PI3K inhibitor Paxalisib, and their combination under IGF2-suppressed conditions. Together, this work provides evidence linking IGF2 expression status with chemoresistance-associated phenotypes, metabolic reprogramming, and PI3K related molecular features in GBM.

Results

Machine learning based integrative analysis identifies cross-hub genes linking metabolic reprogramming and chemoresistance in GBM

To systematically identify key molecular drivers linking metabolic reprogramming to chemoresistance in glioblastoma, we first performed differential expression analysis between TCGA-GBM tumor samples and GTEx normal brain tissues. Using an adjusted P value < 0.05 and $|\log_2 FC| \geq 1$ as significance thresholds, a large set of differentially expressed genes (DEGs) was identified (Fig. 1A), indicating extensive transcriptional remodeling in GBM.

To focus specifically on genes with potential functional relevance to therapy resistance, these DEGs were intersected with curated chemoresistance-associated and metabolic reprogramming-related gene sets. This integrative filtering strategy yielded 120 candidate cross-hub genes (Fig. 1B), representing molecules positioned at the intersection of tumor metabolism and drug resistance.

To further refine this candidate pool, two complementary machine learning approaches were applied. LASSO regression analysis reduced model complexity by penalizing less informative features, resulting in 37 genes with non-zero coefficients at the optimal λ value determined by ten-fold cross-validation (Fig. 1C–D). In parallel, an XGBoost model was constructed to capture nonlinear relationships among candidate genes, and feature importance ranking identified 28 genes with high predictive value (Fig. 1E). Intersection of the LASSO- and XGBoost-derived gene sets yielded 17 consensus hub genes (Fig. 1F), which were selected for subsequent prognostic evaluation and experimental validation.

Prognostic validation in the TCGA and CGGA cohorts identified IGF2 as the most robust survival-associated intersecting hub gene.

To assess the clinical relevance of the 17 machine-learning-derived candidate intersecting hub genes, patients in the TCGA-GBM cohort (n = 166) were dichotomized into high- and low-expression groups according to the median expression of each gene and subjected to Kaplan–Meier OS analysis. Fifteen candidates showed no significant association with OS (Fig. 2A), whereas elevated IGF2 and SFN expression was significantly correlated with poorer OS (Fig. 2B).

Subsequently, we performed external validation of these findings in an independent CGGA cohort comprising 325 samples. The survival association of SFN did not retain statistical significance (P = 0.05), whereas IGF2 remained significantly associated with poor prognosis (P = 0.019) (Fig. 2C). Accordingly, among all candidate genes, IGF2 emerged as the only intersecting hub gene that was consistently and robustly associated with patient survival across both independent cohorts and was therefore selected for subsequent experimental validation and mechanistic analyses.

IGF2 is persistently upregulated in GBM and promotes tumor cell viability

To further delineate the expression landscape of IGF2 in gliomas, we first assessed its expression using publicly available datasets. In the TCGA dataset, IGF2 expression was significantly higher in GBM tumor tissues than in normal brain tissues (Fig. 3A). Consistently, analysis of the CGGA dataset revealed that IGF2 expression was markedly elevated in WHO grade IV gliomas (GBM) compared with WHO grade II and III gliomas (Fig. 3B). Receiver operating characteristic (ROC) curve analysis further demonstrated that IGF2 effectively discriminated tumor from normal tissues, with an area under the curve (AUC) of 0.787 (95% CI: 0.745–0.829) (Fig. 3C), indicating its potential clinical value as a diagnostic biomarker.

We next experimentally validated IGF2 expression in GBM patient samples. Western blot analysis showed higher IGF2 protein levels in tumor tissues relative to normal brain tissues (Fig. 3D), and immunohistochemical staining similarly revealed stronger IGF2-positive signals in tumor sections (Fig. 3E). Following tissue-level validation, we further examined the functional relevance of IGF2 in cellular models. Two independent IGF2 siRNAs were transiently transfected into U87 cells to achieve gene knockdown. Quantitative analyses performed 24 h post-transfection at the mRNA level and 48 h at the protein level confirmed robust downregulation of IGF2, with densitometric analysis of immunoblots yielding consistent results (Fig. 3F-H). Functionally, IGF2 silencing significantly reduced cell viability, as assessed by CCK-8 assays (Fig. 3I), and flow cytometric analysis demonstrated a concomitant increase in apoptotic cells (Fig. 3J).

Collectively, these findings indicate that IGF2 is persistently upregulated in GBM and plays a critical role in maintaining tumor cell viability and survival.

IGF2 regulates a drug resistance associated gene network and tumor metabolic reprogramming in GBM

To elucidate the transcriptional alterations and associated molecular pathways induced by IGF2 silencing, IGF2 was transiently knocked down in U87 cells using siRNA, followed by total RNA extraction and transcriptomic sequencing, as schematically illustrated in Fig. 4A. Differential expression analysis was then performed between the IGF2 knockdown and control groups, and the resulting differentially expressed genes (DEGs) were visualized accordingly (Fig. 4B). A heatmap highlighted the differential expression patterns of drug resistance–related genes (Fig. 4C).

Concurrently, correlation analysis in the TCGA-GBM cohort revealed significant positive correlations between IGF2 expression and multiple drug resistance–associated genes (Fig. 4D), suggesting that high IGF2 expression is accompanied by a transcriptional program linked to therapeutic resistance in GBM. Furthermore, gene set enrichment analysis (GSEA) demonstrated significant enrichment of pathways related to DNA damage repair, cellular metabolism, and cell cycle regulation (Padj < 0.05). These transcriptomic findings indicate that IGF2 knockdown concomitantly affects the expression of drug resistance–associated genes and multiple metabolic pathways, providing a mechanistic basis for subsequent functional and pathway-level investigations.

IGF2 expression status is associated with drug resistance related phenotypes and PI3K pathway associated transcriptional signatures

To investigate IGF2-associated signaling pathways at the clinical cohort level, tumor samples from the TCGA-GBM cohort were stratified into high- and low-IGF2 expression groups based on the median IGF2 expression level. Differential expression analysis identified 649 upregulated genes and 259 downregulated genes between the two groups (Fig. 5A). Subsequent KEGG pathway enrichment analysis revealed significant enrichment of multiple cancer-related signaling pathways, among which the PI3K-

AKT signaling pathway emerged as one of the most significantly enriched terms (Fig. 5B), suggesting a close association between high IGF2 expression and PI3K-Akt pathway activity. In parallel, GO and KEGG enrichment analyses of transcriptomic data from IGF2-silenced U87 cells likewise identified PI3K-related signaling pathways among the significantly enriched categories (Fig. 5C), providing independent support for the pathway enrichment results derived from the TCGA cohort. A chord diagram further highlighted genes associated with PI3K pathway terms and their directions of change (Fig. 5D).

For functional validation, we first assessed whether IGF2 knockdown affects the sensitivity of U87 cells to temozolomide (TMZ). Under siIGF2 conditions, TMZ treatment (200 μM, 24 h) induced a more pronounced reduction in cell viability compared with control cells, indicating that IGF2 knockdown enhances TMZ sensitivity in U87 cells (Fig. 5E). We next evaluated the effect of the PI3K inhibitor paxalisib on cell viability. In vitro treatment with paxalisib (1 μM, 24 h) significantly reduced U87 cell viability (Fig. 5F). Based on these findings, to compare the effects of single-agent versus combination treatment on cell viability under IGF2-silenced conditions, we selected the more effective siIGF2#2 and examined TMZ, paxalisib, and their combination. Paxalisib treatment resulted in a greater reduction in cell viability than TMZ alone, and combined treatment with TMZ and paxalisib further decreased cell viability. Notably, under IGF2 knockdown conditions, cell viability in the TMZ plus paxalisib group was reduced by approximately 15% compared with paxalisib alone and by approximately 35% compared with TMZ alone (Fig. 5G).

Taken together, both the differential expression analysis of IGF2 stratified TCGA samples and the enrichment analysis of IGF2 knockdown transcriptomes consistently point to PI3K-related transcriptional features. The corresponding cellular assays demonstrate that, upon IGF2 downregulation, TMZ or paxalisib treatment leads to a more pronounced reduction in cell viability than monotherapy, with the most substantial effect observed with combined TMZ and paxalisib treatment. These findings suggest that IGF2 expression status is associated with TMZ resistance and PI3K-related molecular characteristics in GBM.

Discussion

In this study, we systematically characterized IGF2-associated molecular features across multiple public cohorts, patient-derived specimens, and cellular models. Consistent differences in IGF2 expression were observed at both the transcript and protein levels, and functional as well as transcriptional changes accompanied modulation of IGF2 expression in vitro. Collectively, these findings suggest that IGF2 expression is closely associated with TMZ resistance–related phenotypes and metabolic reprogramming linked transcriptional programs in GBM, thereby providing a focused entry point for subsequent mechanistic investigation.

At the cellular level, IGF2 downregulation was accompanied by reduced cell viability and increased apoptotic fractions, indicating a role for IGF2 in maintaining GBM cell survival. Under TMZ treatment, cells with reduced IGF2 expression exhibited a more pronounced decrease in viability, supporting an

association between IGF2 status and TMZ responsiveness. Transcriptomic profiling further revealed that IGF2 knockdown was associated with coordinated alterations in pathways related to DNA damage repair, cell-cycle regulation, and cellular metabolism, along with an overall downregulation trend of resistance-associated genes. Importantly, these observations primarily reflect transcript-level associations and pathway-level enrichment patterns, which should be interpreted as molecular correlates linked to IGF2 expression rather than evidence of a single, linear causal mechanism.

Notably, pathway enrichment analyses derived from both IGF2-based stratification in patient cohorts and transcriptomic profiling following IGF2 knockdown consistently highlighted PI3K-related transcriptional signatures. Guided by this convergent signal, we further examined the effects of the PI3K inhibitor Paxalisib, TMZ, and their combination on cell viability under conditions of IGF2 downregulation. Paxalisib alone significantly reduced cell viability, with a more pronounced effect observed when IGF2 expression was suppressed. Using the most effective siIGF2 strategy, we found that Paxalisib induced a greater reduction in viability than TMZ, and that combined treatment with Paxalisib and TMZ resulted in a further decrease in cell viability. Together, these findings suggest that IGF2 expression status may be linked to both TMZ resistance and PI3K-associated molecular features, and that targeting the IGF2–PI3K axis may influence therapeutic responsiveness in GBM.

Several limitations of the present study should be acknowledged. First, the pathway-level evidence presented here is largely based on differential expression and enrichment analyses, and direct validation of key signaling nodes at the protein and functional levels is currently lacking. Therefore, the conclusions should be confined to an association- and hypothesis-generating framework. Future studies incorporating phosphorylation assays, upstream perturbation, and rescue experiments will be essential to establish causality. Second, the evaluation of combined TMZ and Paxalisib treatment was primarily based on cell viability measurements. A more comprehensive characterization of their interaction will require systematic dose–response analyses and quantitative synergy assessment. Third, this study focused mainly on tumor cell–intrinsic changes and did not address potential roles of IGF2 in the tumor microenvironment, which represents an important direction for future investigation.

In summary, our integrative analyses and functional experiments identify IGF2 as a molecular factor associated with adverse prognosis, resistance-related transcriptional features, and metabolic pathway alterations in GBM. These findings provide a conceptual framework for future mechanistic studies and suggest that modulation of the IGF2-PI3K axis may represent a promising avenue for therapeutic sensitization strategies.

Materials and Methods

Acquisition and preprocessing of TCGA datasets

RNA-seq raw count matrices and corresponding clinical information for TCGA glioblastoma (TCGA-GBM) tumor samples were downloaded from the TCGA data portal (https://portal.gdc.cancer.gov/)[16]. RNA-

seq data for normal brain tissues were obtained from the Genotype-Tissue Expression (GTEx) project (https://gtexportal.org/)[17]. Glioma cohort data used for external survival validation were accessed via the online analysis platform of the Chinese Glioma Genome Atlas (CGGA; https://www.cgga.org.cn/)[18]. Gene sets related to drug resistance (Relevance score > 2) and metabolic reprogramming (Relevance score > 1) were retrieved from GeneCards (https://www.genecards.org/)[19].

All bioinformatic analyses were performed using R software (version 4.3.3). After quality control and missing value processing, a total of 166 GBM tumor samples and 1,152 normal brain tissue samples were included for subsequent analyses. Expression matrices from TCGA and GTEx were merged, and batch effects were corrected using the ComBat algorithm implemented in the *sva* package.

Correlation and differential expression analyses

Correlation analyses were conducted in TCGA-GBM tumor samples using Spearman's rank correlation to evaluate the associations between *IGF2* expression and resistance-related genes. Differential expression analysis based on TCGA data was performed using the *DESeq2* package, whereas differential expression analysis of in-house RNA-seq data was conducted using the *limma* package. Genes with $|\log_2$ fold change (FC)$| \geq 1$ and Benjamini–Hochberg (BH)–adjusted P values < 0.05 were considered significantly differentially expressed. Volcano plots were generated using the *ggplot2* package to visualize differential expression results.

Pathway enrichment analysis and gene set enrichment analysis (GSEA)

Gene Ontology (GO) and Kyoto Encyclopedia of Genes and Genomes (KEGG) pathway enrichment analyses were performed using the *clusterProfiler* package. GSEA was conducted using *clusterProfiler* based on gene sets downloaded from the Molecular Signatures Database (MSigDB). Enrichment scores were calculated on ranked gene lists, and enrichment curves were generated accordingly. A BH-adjusted P value (Padj) < 0.05 was used as the threshold for statistical significance in GSEA.

Identification of cross-hub genes and machine learning based feature selection

Intersections among gene sets were visualized using Venn diagrams generated with the *VennDiagram* package. Least absolute shrinkage and selection operator (LASSO) regression was implemented using the *glmnet* package. Ten-fold cross-validation was applied to determine the optimal penalty parameter (λ), and genes with non-zero coefficients were retained. The XGBoost model was constructed using the *xgboost* package, with five-fold cross-validation applied to assess model stability and feature importance. Candidate genes were selected based on a gain value > 0.01. The intersection of genes

identified by LASSO and XGBoost was defined as the consensus candidate gene set and used for subsequent survival analyses and experimental validation.

Survival analysis

For the TCGA cohort, gene expression data and overall survival information of GBM patients were extracted. Patients were divided into high- and low-expression groups according to the median expression level of each candidate gene. Kaplan–Meier survival curves were generated using the *survival* and *survminer* packages, and differences between groups were evaluated using the log-rank test. A P value < 0.05 was considered statistically significant. Kaplan–Meier survival analyses for the CGGA cohort were performed using the online survival analysis tool provided by the CGGA website for external validation.

ROC analysis and visualization of transcriptomic results

Receiver operating characteristic (ROC) curve analysis was performed to assess the ability of *IGF2* to discriminate tumor samples (TCGA-GBM, n = 166) from normal brain tissues (GTEx, n = 1,152). The area under the curve (AUC) and corresponding 95% confidence intervals were calculated using the *pROC* package. Differential gene expression patterns were visualized using heatmaps generated with the *pheatmap* package. Associations between pathway-related genes and differentially expressed genes were visualized using chord diagrams generated with the *circlize* package.

Cell culture

The human glioblastoma cell line U87 was obtained from the Cell Bank of the Chinese Academy of Sciences (Shanghai, China). Cells were cultured in Dulbecco's modified Eagle's medium (DMEM; Gibco) supplemented with 10% fetal bovine serum and penicillin–streptomycin (final concentrations: 100 U/mL penicillin and 100 μg/mL streptomycin; Gibco). Cells were maintained at 37°C in a humidified incubator with 5% CO_2.

Transient siRNA transfection

U87 cells were seeded in 6-well plates and transfected at approximately 60%–70% confluence using CALNP™ RNAi Transfection Reagent (D-Nano Therapeutics, Beijing, China). *IGF2* siRNAs were transfected at a final concentration of 50 nM, with a negative control siRNA (siNC; Qingke Biotechnology, Beijing, China) included as a control. Fresh culture medium was replaced 24 h after transfection. Cells were harvested at 24 h post-transfection for qRT-PCR analysis and at 48 h for Western blotting and subsequent functional assays.

The sequences of *IGF2* siRNAs were as follows:

si*IGF2*-1[20]: sense 5'-GAAGUCGAUGCUGGUGCUUTT-3'; antisense 5'-AAGCACCAGCAUCGACUUCTT-3'.
si*IGF2*-2[21]: sense 5'-CGCAGCACAUACAUGAACATT-3'; antisense 5'-UGUUCAUGUAUGUGCUGCGTT-3'

RNA extraction and quantitative real-time PCR

Total RNA was extracted using TRIzol reagent (Invitrogen, USA) and reverse-transcribed into cDNA using a reverse transcription kit (Vazyme, China). Quantitative real-time PCR was performed using AceQ SYBR Green Mix (Vazyme, China), with GAPDH used as the internal control. Relative gene expression levels were calculated using the $2^{-}\Delta\Delta Ct$ method. The primer sequences for *IGF2* were as follows21:

Forward: 5'-GTGGCATCGTTGAGGAGTG-3'

Reverse: 5'-CACGCCCTCTCGGACTTG-3'

Western blot analysis

Cells were lysed using RIPA buffer supplemented with phosphatase inhibitors and PMSF (Solarbio, Beijing, China). Lysates were centrifuged at 12,000 rpm for 15 min at 4°C, and protein concentrations were determined using a BCA assay kit (Solarbio). Equal amounts of protein were mixed with 5× SDS-PAGE loading buffer, denatured at 100°C for 10 min, separated by 10% SDS-PAGE, and transferred onto Immobilon-P PVDF membranes (Millipore, USA). Membranes were blocked at room temperature for 10 min and incubated with primary antibodies overnight at 4°C. Primary antibodies included anti-IGF2 (ABclon, Wuhan, China; 1:500) and anti-GAPDH (HUABIO) as a loading control. After incubation with HRP-conjugated secondary antibodies (HUABIO) for 1 h at room temperature, protein bands were detected using a ChemiDoc imaging system (Bio-Rad, USA). Band intensities were quantified using ImageJ software and normalized to GAPDH.

Immunohistochemistry

GBM tumor tissues and normal brain tissues (n = 4 per group) were obtained from the Affiliated Central Hospital of Dalian University. The study was approved by the institutional ethics committee (Approval No. YN2024-022-03). Paraffin-embedded tissue sections were deparaffinized, rehydrated, and subjected to antigen retrieval in citrate buffer (pH 6.0), followed by endogenous peroxidase blocking (ZSGB-BIO, Beijing, China). Sections were incubated with anti-IGF2 primary antibody (ABclon; 1:100) overnight at 4°C, followed by incubation with enzyme-labeled polymer secondary antibody (ZSGB-BIO) at 37°C for 20 min. Color development was performed using a DAB substrate kit (ZSGB-BIO), followed by hematoxylin counterstaining, dehydration, mounting, and image acquisition.

Cell viability assays and drug treatments

U87 cells were seeded in 96-well plates at a density of 1×10^4 cells per well and allowed to adhere overnight. For TMZ sensitivity assays, cells were treated with TMZ (200 μM) for 24 h. For PI3K–mTOR inhibition experiments, cells were treated with TMZ (200 μM), Paxalisib (1 μM), or a combination of both for 24 h. All drugs were prepared according to the manufacturers' instructions, and equivalent volumes of solvent were used as controls when necessary. After treatment, CCK-8 reagent (10 μL; Solarbio) was added to each well and incubated at 37°C for 30 min. Absorbance was measured at 450 nm to assess cell viability. Each condition was tested in at least three technical replicates and repeated in at least three independent experiments.

RNA sequencing sample preparation and sequencing

U87 cells were harvested 48 h after transfection with si*IGF2*-2, with non-transfected cells used as controls. Total RNA was extracted using TRIzol, and three biological replicates were included per group. RNA quality control, library preparation, and paired-end 150 bp sequencing were performed by a commercial service provider (Heyuan Biotechnology, Shanghai, China) using the Illumina NovaSeq 6000 platform.

Annexin V and PI apoptosis assay

U87 cells were seeded in 6-well plates at a density of 2.5×10^5 cells per well and allowed to adhere overnight. After siRNA transfection, cells were harvested at the indicated time points. Apoptosis was assessed using an Annexin V-FITC/PI apoptosis detection kit (Solarbio, Beijing, China) according to the manufacturer's instructions. Cells were resuspended in 200 μL binding buffer, stained with Annexin V-FITC and PI, and incubated for 15 min at room temperature in the dark. Samples were analyzed using a flow cytometer (Aurora, Cytek, USA).

Statistical analysis

All statistical analyses were performed using R software (version 4.3.3) and GraphPad Prism (version 10.0.0). Data are presented as mean ± standard deviation (SD) and were obtained from at least three independent experiments. Comparisons between two groups were performed using two-tailed Student's *t* tests. Correlations between gene expression levels were assessed using Spearman's correlation analysis. Survival curves were generated using the Kaplan–Meier method and compared using the log-rank test. A P value < 0.05 was considered statistically significant, with significance levels indicated as *P* < 0.05, **P** < 0.01, **P** < 0.001, and **P** < 0.0001.

Declarations

Acknowledgements

The authors would like to thank the members of the Wu laboratory at the Shandong Laboratory of Yantai Drug Discovery, Bohai Rim Advanced Research Institute for Drug Discovery, for their technical assistance and helpful discussions.

Author contributions

All authors contributed to this study. Wenrui Jin: Investigation, Methodology, Validation, Data curation, Visualization and Writing-Original Draft. Zefeng Song: Methodology and Validation, Investigation, Data curation and Visualization. Xiaojing Zhu: Investigation, Data curation and Visualization. Yutong Xing: Methodology and Validation. Kai Xu: Methodology, Investigation. Haoran Geng: Methodology, Investigation. Peng Zhang: Methodology, Investigation, Conceptualization. Chengjun Wu: Methodology,

Investigation, Conceptualization. Zhenyong Wu: Supervision, Conceptualization, Funding acquisition and Writing-Review & Editing.

Funding

This work was financially supported by the Key Projects of the Yantai Science and Technology Innovation Development Plan (2024JCYJ059), the Key R&D Program of Shandong Province, China (2024CXPT029), the National Natural Science Foundation of China (No. 32371283), the Taishan Scholars Program (2023000027), the Special Supporting Funds for Leading Talents at or Above the Provincial Level in Yantai City (2023000090).

Data availability

Data will be made available on request.

Ethical approval All methods were carried out in accordance with relevant guidelines and regulations. The use of human GBM and normal brain tissue specimens in this study was approved by the institutional ethics committee of the Affiliated Central Hospital of Dalian University (Approval No. YN2024-022-03).

Competing interests

The authors declare no conflicts of competing interest.

References

1. (2013) The Genotype-Tissue Expression (GTEx) project. Nat Genet 45:580-585. DOI 10.1038/ng.2653
2. Agnihotri S, et al. (2016) Metabolic reprogramming in glioblastoma: the influence of cancer metabolism on epigenetics and unanswered questions. Neuro Oncol 18:160-172. DOI 10.1093/neuonc/nov125
3. Cortes Ballen AI, et al. (2024) Metabolic Reprogramming in Glioblastoma Multiforme: A Review of Pathways and Therapeutic Targets. Cells 13. DOI 10.3390/cells13181574
4. Heath AP, et al. (2021) The NCI Genomic Data Commons. Nat Genet 53:257-262. DOI 10.1038/s41588-021-00791-5
5. Hegi ME, et al. (2015) Withholding temozolomide in glioblastoma patients with unmethylated MGMT promoter--still a dilemma? Neuro Oncol 17:1425-1427. DOI 10.1093/neuonc/nov198
6. Jang HJ, et al. (2024) Tobacco-induced hyperglycemia promotes lung cancer progression via cancer cell-macrophage interaction through paracrine IGF2/IR/NPM1-driven PD-L1 expression. Nat Commun 15:4909. DOI 10.1038/s41467-024-49199-9
7. Ji J, et al. (2024) Single-cell transcriptome analysis revealed heterogeneity in glycolysis and identified IGF2 as a therapeutic target for ovarian cancer subtypes. BMC Cancer 24:926. DOI

10.1186/s12885-024-12688-7

8. Kitange GJ, et al. (2009) Induction of MGMT expression is associated with temozolomide resistance in glioblastoma xenografts. Neuro Oncol 11:281-291. DOI 10.1215/15228517-2008-090
9. LeRoith D, et al. (2021) Insulin-like growth factors: Ligands, binding proteins, and receptors. Mol Metab 52:101245. DOI 10.1016/j.molmet.2021.101245
10. Li H, et al. (2025) Overcoming temozolomide resistance in glioma: recent advances and mechanistic insights. Acta Neuropathol Commun 13:126. DOI 10.1186/s40478-025-02046-4
11. Livingstone C (2013) IGF2 and cancer. Endocr Relat Cancer 20:R321-339. DOI 10.1530/erc-13-0231
12. Omuro A, et al. (2013) Glioblastoma and other malignant gliomas: a clinical review. Jama 310:1842-1850. DOI 10.1001/jama.2013.280319
13. Roos WP, et al. (2007) Apoptosis in malignant glioma cells triggered by the temozolomide-induced DNA lesion O6-methylguanine. Oncogene 26:186-197. DOI 10.1038/sj.onc.1209785
14. Stelzer G, et al. (2016) The GeneCards Suite: From Gene Data Mining to Disease Genome Sequence Analyses. Curr Protoc Bioinformatics 54:1.30.31-31.30.33. DOI 10.1002/cpbi.5
15. Wang X, et al. (2025) Asparagine endopeptidase prompts breast cancer-related pericardial calcification by regulating IGF2 and integrin αvβ5. Proc Natl Acad Sci U S A 122:e2512936122. DOI 10.1073/pnas.2512936122
16. Weller M, et al. (2013) Standards of care for treatment of recurrent glioblastoma--are we there yet? Neuro Oncol 15:4-27. DOI 10.1093/neuonc/nos273
17. Wu W, et al. (2021) Glioblastoma multiforme (GBM): An overview of current therapies and mechanisms of resistance. Pharmacol Res 171:105780. DOI 10.1016/j.phrs.2021.105780
18. Xu X, et al. (2023) Metabolic reprogramming and epigenetic modifications in cancer: from the impacts and mechanisms to the treatment potential. Exp Mol Med 55:1357-1370. DOI 10.1038/s12276-023-01020-1
19. Yang Q, et al. (2018) Direct repression of IGF2 is implicated in the anti-angiogenic function of microRNA-210 in human retinal endothelial cells. Angiogenesis 21:313-323. DOI 10.1007/s10456-018-9597-6
20. Zhang J, et al. (2023) Cancer-associated fibroblasts potentiate colorectal cancer progression by crosstalk of the IGF2-IGF1R and Hippo-YAP1 signaling pathways. J Pathol 259:205-219. DOI 10.1002/path.6033
21. Zhao Z, et al. (2021) Chinese Glioma Genome Atlas (CGGA): A Comprehensive Resource with Functional Genomic Data from Chinese Glioma Patients. Genomics Proteomics Bioinformatics 19:1-12. DOI 10.1016/j.gpb.2020.10.005

Figures

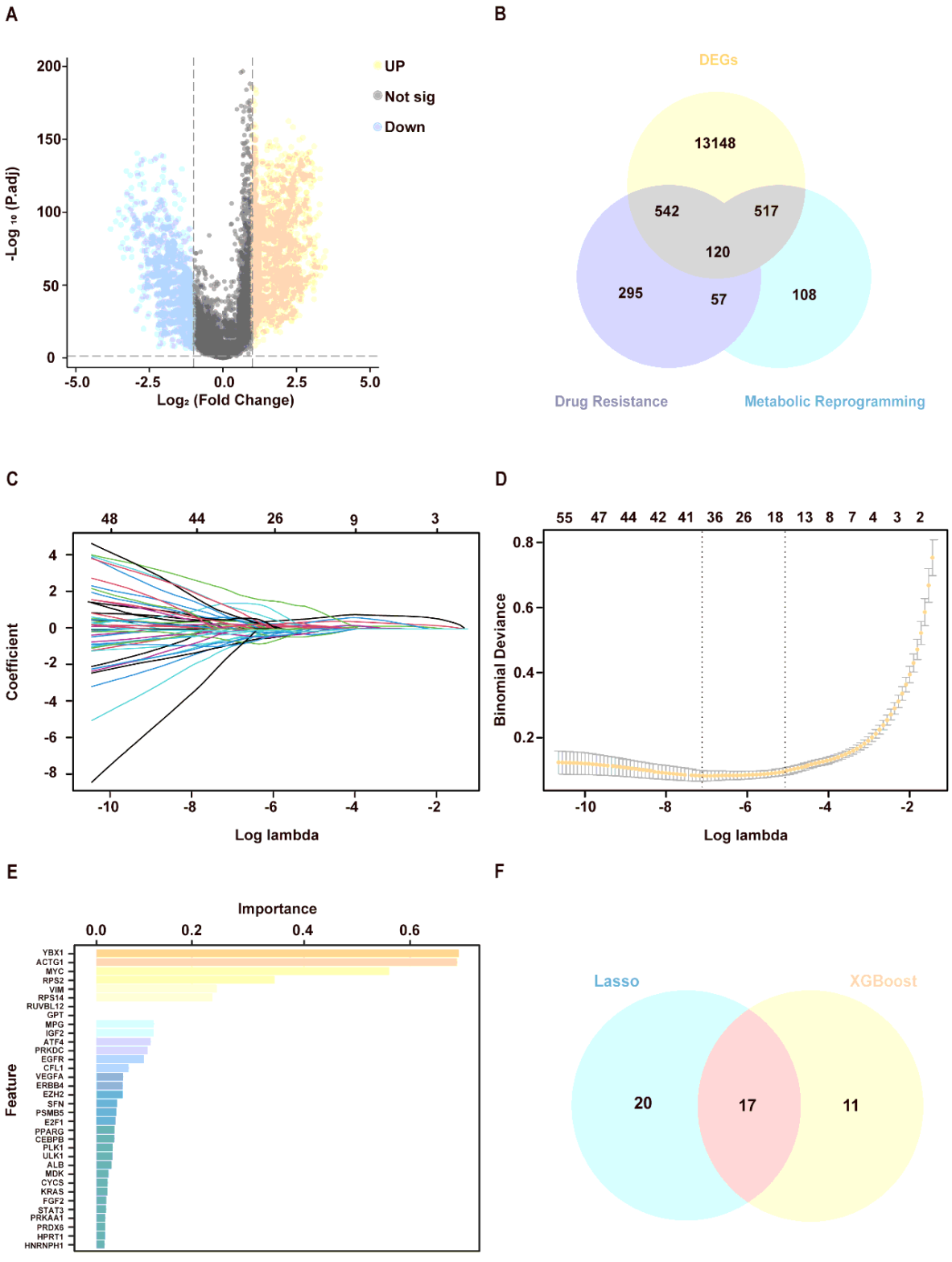


Figure 1

Integrated machine-learning analysis identifies cross-hub genes linking metabolic reprogramming and chemoresistance in GBM

(A)Volcano plot showing differentially expressed genes between TCGA-GBM tumor samples and GTEx normal brain tissues. Significance thresholds were set at adjusted P < 0.05 and |$\log_2$ fold change| ≥ 1. (B)

Venn diagram illustrating the intersection of differentially expressed genes with chemoresistance-associated gene sets and metabolic reprogramming–related gene sets, yielding 120 candidate cross-hub genes.(C–D) LASSO regression analysis based on the 120 candidate genes. The coefficient path plot and ten-fold cross-validation curve were used to determine the optimal penalty parameter λ, resulting in the selection of 37 genes with non-zero coefficients.
(E) XGBoost model constructed using the same candidate gene set with cross-validation. Twenty-eight genes were prioritized based on feature importance scores. (F) Intersection analysis of genes identified by LASSO and XGBoost, yielding 17 consensus cross-hub genes for subsequent clinical correlation analyses and experimental validation.

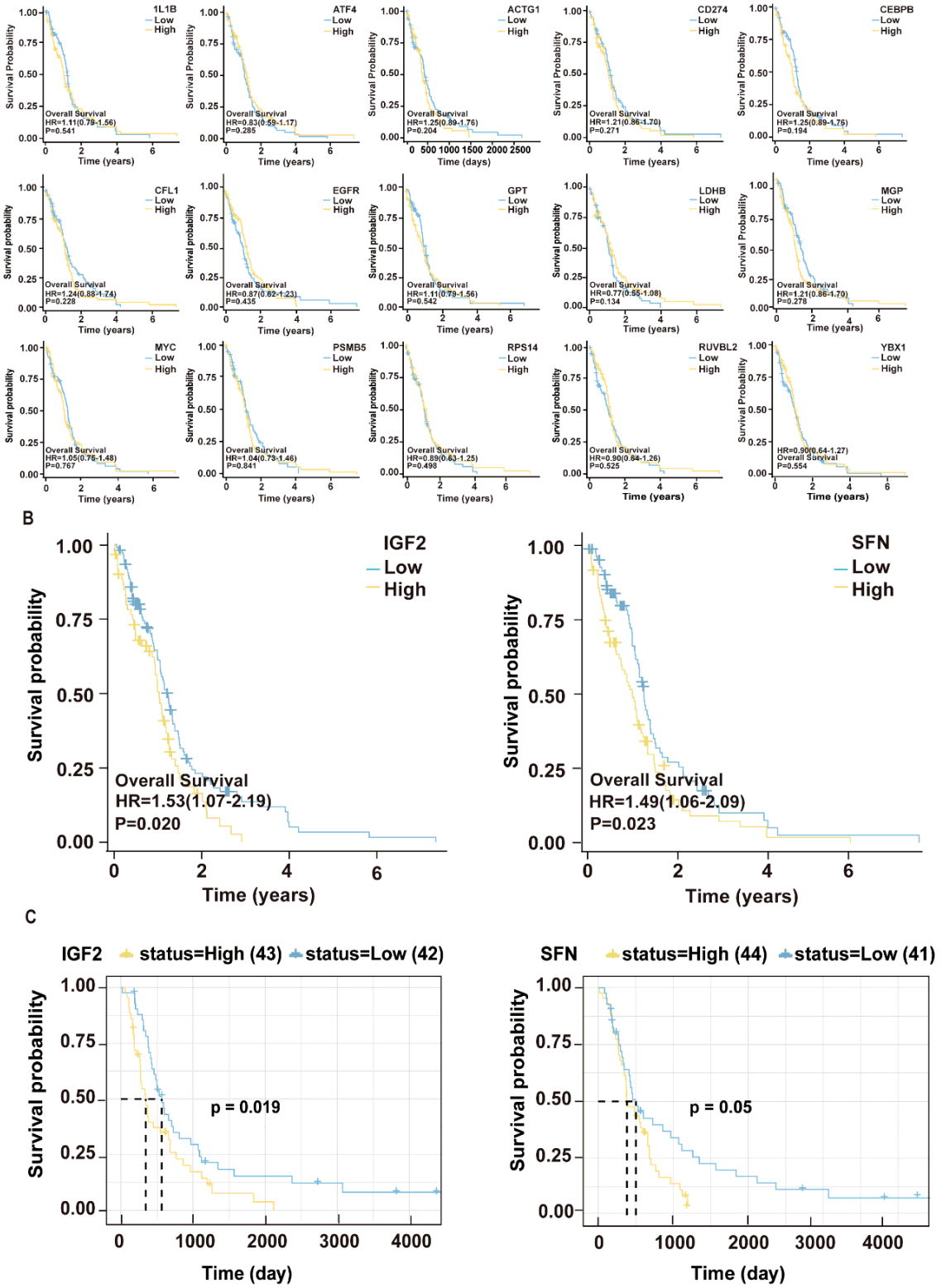


Figure 2

Cross-cohort survival validation identifies IGF2 as the most robust survival-associated candidate gene

(A)Kaplan–Meier overall survival analysis of the 17 candidate genes in the TCGA-GBM cohort (n = 166), showing that 15 genes were not significantly associated with overall survival. (B) Kaplan–Meier overall survival curves for IGF2 and SFN in the TCGA-GBM cohort. High expression of either gene was

associated with significantly shorter overall survival compared with the low-expression group. (C) External validation of IGF2 and SFN in an independent CGGA cohort. SFN failed to maintain statistical significance (P = 0.05), whereas *IGF2* remained significantly associated with poor prognosis (P = 0.019).

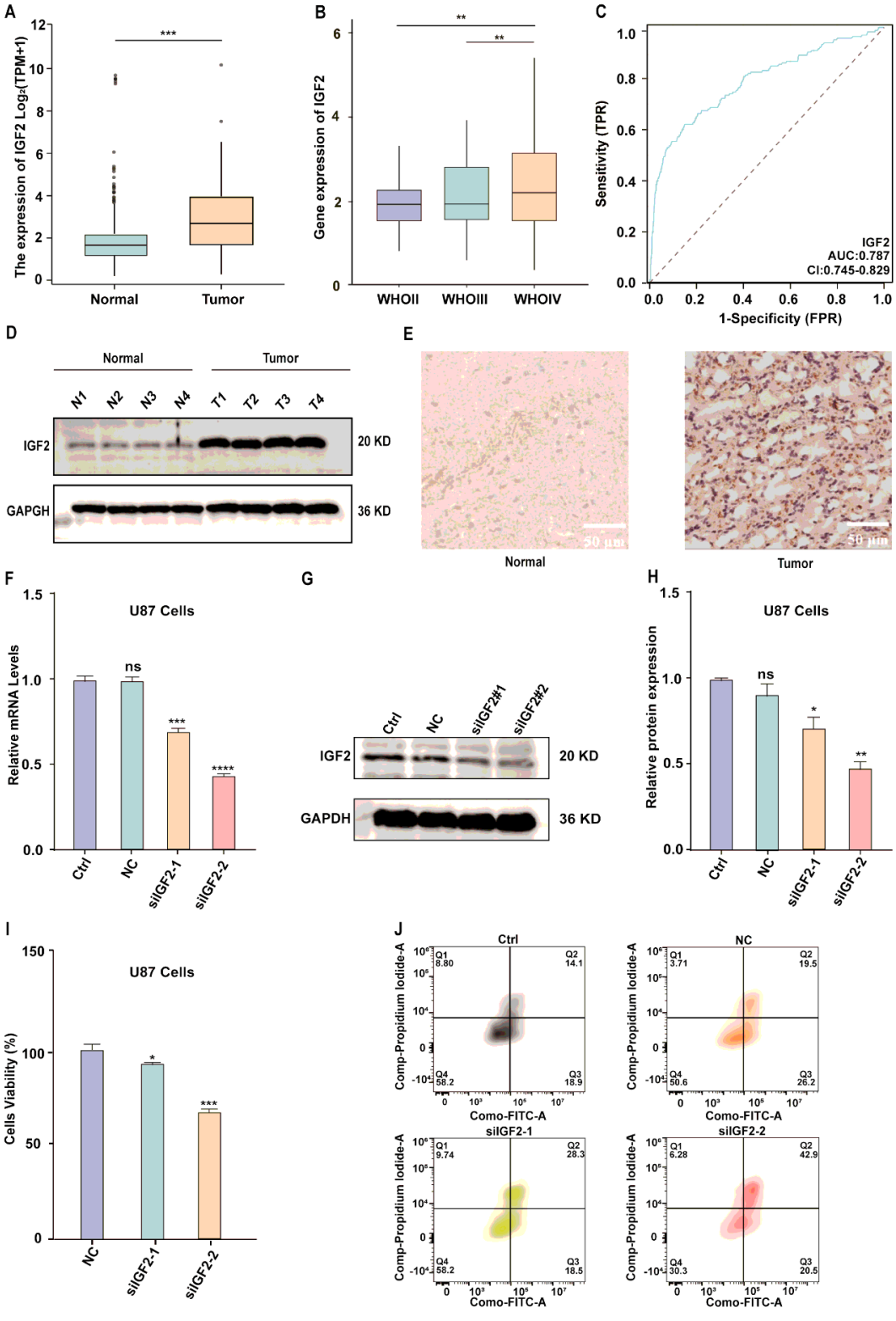


Figure 3

IGF2 is persistently upregulated in GBM and correlates with tumor cell proliferation and survival

(A)Differential expression of IGF2 between GBM tumor tissues and normal brain tissues in the TCGA dataset. (B) Comparison of IGF2 expression across different glioma grades in the CGGA dataset, showing significantly higher expression in grade IV gliomas (GBM) than in grades II and III. (C) Receiver operating characteristic (ROC) curve evaluating the ability of *IGF2* to distinguish tumor from normal tissues, with an AUC of 0.787 (95% CI: 0.745–0.829). (D) Western blot analysis of IGF2 protein expression in patient-derived tissue samples.(E) Immunohistochemical staining showing IGF2 expression and staining intensity in GBM tumor tissues compared with normal brain tissues. (F) qRT-PCR validation of IGF2 mRNA knockdown 24 h after transient transfection of U87 cells with two independent *IGF2* siRNAs. (G) Western blot validation of IGF2 protein knockdown 48 h after transfection. (H) Densitometric quantification of IGF2 protein levels shown in (G). (I) CCK-8 assay assessing changes in U87 cell viability following IGF2 knockdown. (J) Annexin V and propidium iodide flow cytometry analysis of apoptosis in U87 cells after IGF2 knockdown.

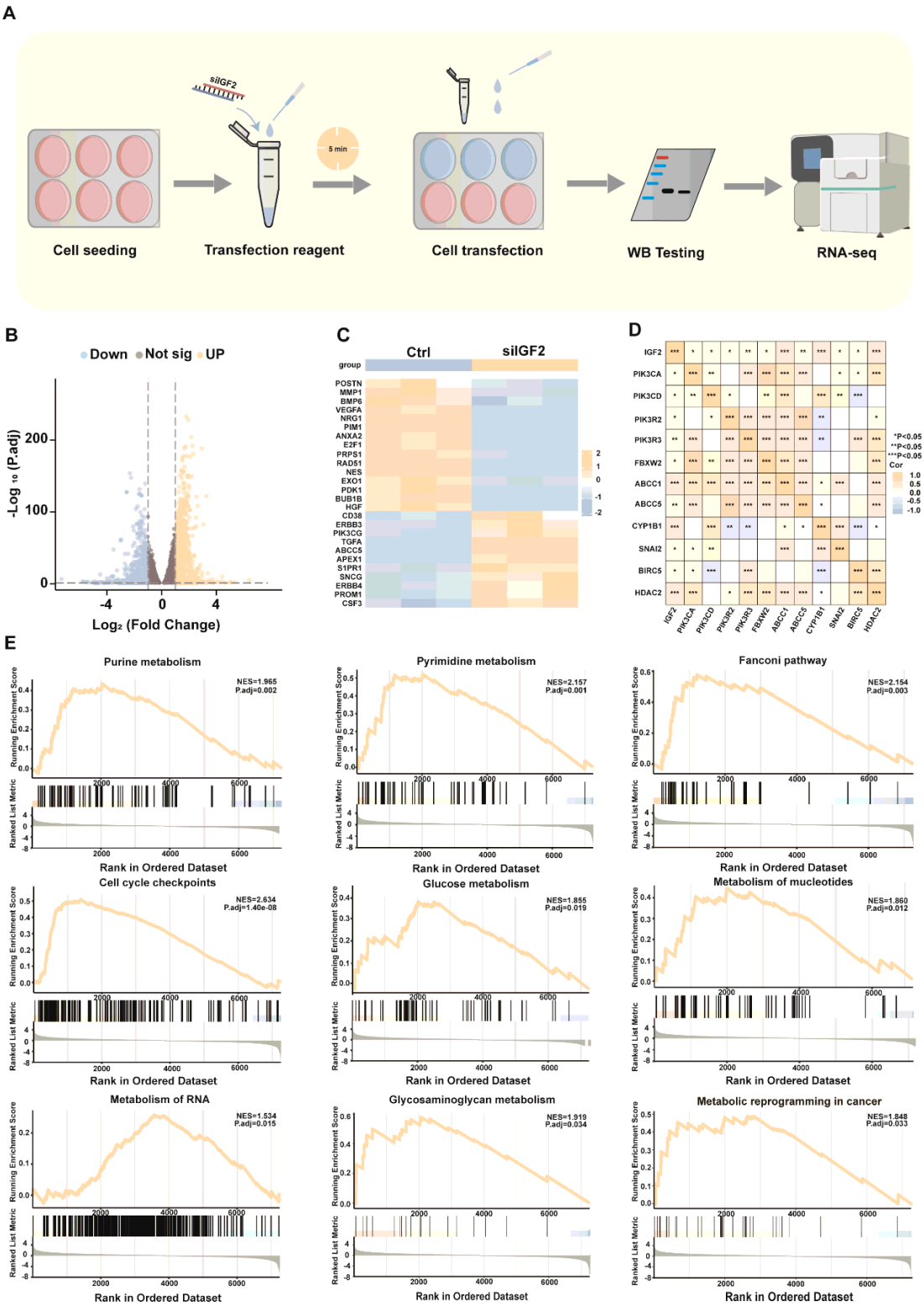


Figure 4

IGF2 knockdown induces coordinated alterations in resistance-related gene expression and metabolic pathway enrichment

(A)Schematic overview of the experimental workflow for transcriptomic profiling following transient IGF2 knockdown in U87 cells, including RNA extraction and RNA-seq analysis. (B) Visualization of

differentially expressed genes identified by RNA-seq analysis between IGF2 knockdown and control groups. (C) Heatmap of differentially expressed chemoresistance-related genes showing global expression changes following IGF2 knockdown. Resistance-associated genes were curated from GeneCards and filtered for analysis. (D) Spearman correlation analysis in the TCGA-GBM cohort demonstrating positive correlations between IGF2 expression and resistance-related genes in tumor samples. (E) Gene Set Enrichment Analysis (GSEA) based on ranked differential expression lists, revealing significant enrichment of pathways related to DNA damage repair, cellular metabolism, and cell-cycle regulation (adjusted $P < 0.05$). Representative enrichment plots are shown.

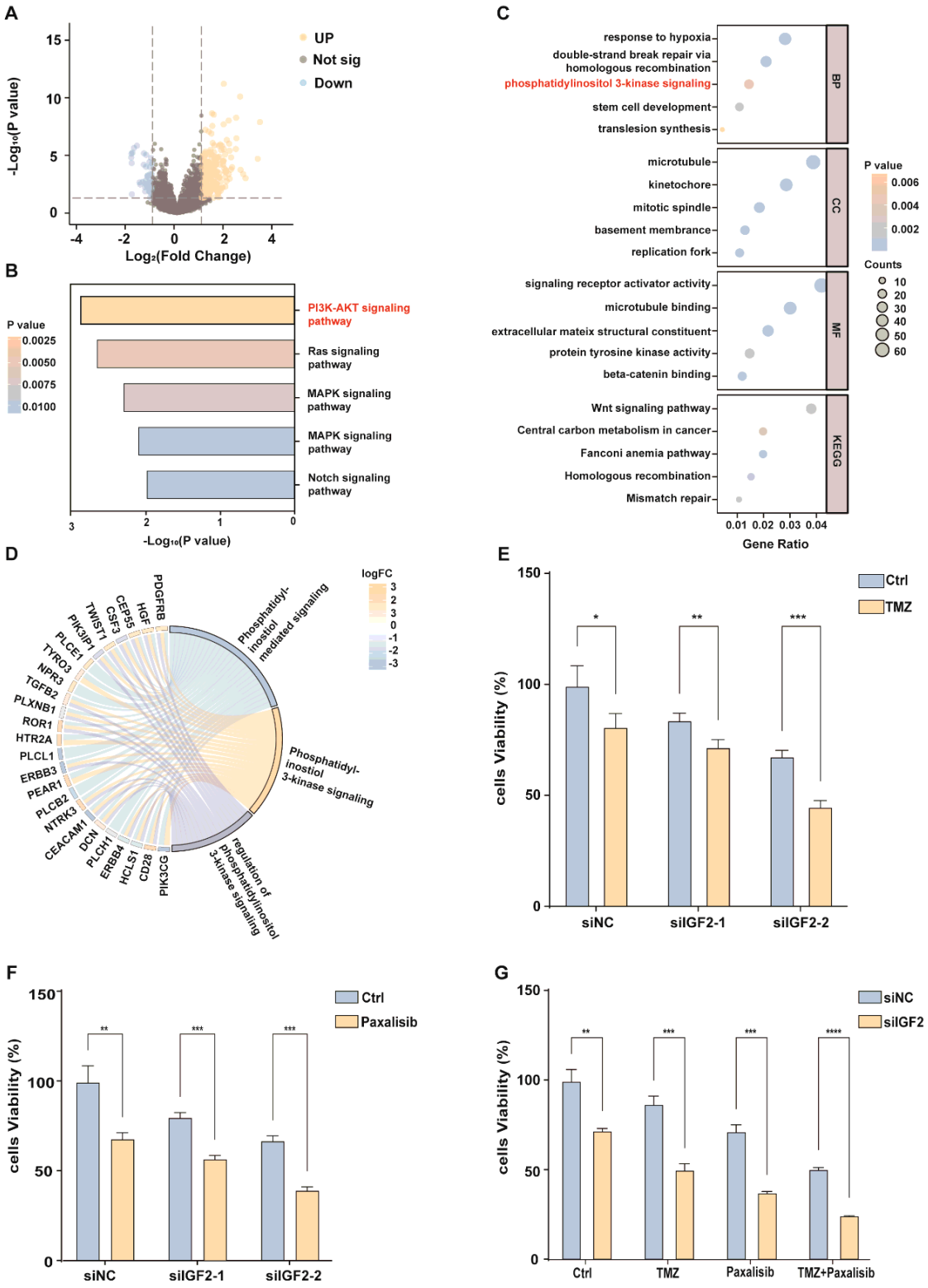


Figure 5

Validation of the association between IGF2, chemoresistance phenotypes, and PI3K pathway activation

(A) Volcano plot of differentially expressed genes between *IGF2*-high and *IGF2*-low groups in the TCGA-GBM cohort, stratified by median *IGF2* expression. (B) KEGG pathway enrichment analysis of differentially expressed genes shown in (A), identifying the PI3K signaling pathway as one of the

significantly enriched pathways. (C) Bubble plot of pathway enrichment analysis based on RNA-seq differential genes from IGF2-knockdown U87 cells, showing significant enrichment of PI3K-related pathways. (D) Chord diagram illustrating the relationships between significantly altered genes following IGF2 knockdown and the PI3K signaling pathway. (E) CCK-8 assay evaluating the effect of IGF2 knockdown on cell viability under TMZ treatment (200 μM, 24 h). TMZ-induced reduction in cell viability was significantly enhanced in the si*IGF2* group compared with controls. (F) CCK-8 assay assessing the effect of the PI3K inhibitor Paxalisib (1 μM, 24 h) on U87 cell viability. (G) Comparison of cell viability under control, TMZ, Paxalisib, and combined TMZ plus Paxalisib treatments in siIGF2-2-transfected cells. Within the same treatment window, Paxalisib induced a greater reduction in cell viability than TMZ alone, and the combination treatment further enhanced cytotoxicity.